EVALUATION OF THE APPROACHING TRAJECTORIES FOR LANDING ON THE ASTEROID 216 KLEOPATRA

Evandro Marconi Rocco
evandro.rocco@inpe.br
Instituto Nacional de Pesquisas Espaciais – INPE
C.P. 515 CEP 12201-970 – São José dos Campos, SP, Brasil

Abstract. The goal of this work is to evaluate some orbital trajectories seeking the approaching for landing on surface of the asteroid 216 Kleopatra. This asteroid, discovered by Johann Palisa in 1880, has a very irregular shape with approximate dimensions of 217 x 94 x 81 km. Due to its shape, the gravitational field around the asteroid cannot be considered central. Thus, a spacecraft approaching the asteroid is subject to orbital perturbations, which can hinder the vehicle to describe the nominal trajectory. In maneuvers for approach and landing, the trajectory deviations may result in very high approach velocities, making impossible the soft landing on the surface of the asteroid. In addition, the rotation of the asteroid is another difficulty for missions aimed at the soft landing. Due to the irregular shape of the asteroid the relative distance between the surface and the spacecraft varies significantly depending on the orbital plane adopted for the trajectory. In this work, the intention is to evaluate, through numerical simulations, orbits of a spacecraft around the asteroid Kleopatra more appropriate to get closer to the asteroid in order to minimize the relative velocity between the surface and the spacecraft. For this, was used a polyhedral model of the asteroid's volume, based on radar measurements from the Arecibo Observatory, to model the non-central gravitational field generated by the heterogeneous mass distribution of the asteroid. Using the model of the gravitational field and the simulation environment Spacecraft Trajectory Simulator (STRS), several approach paths were simulated and compared in order to assist the choice of trajectories, considering the minimum value for the velocity with respect to the surface at the point of the trajectory with minimum altitude.

Keywords: Astrodynamics, Orbital Motion, Orbital Maneuver, Asteroid Kleopatra, Irregular Bodies.

1   Introduction

Orbiting a body with irregular mass distribution like an asteroid is a major challenge due to the difficulty in modelling of the gravitational field around that body. In many cases the mass distribution of the asteroid is nothing like a spherical body, preventing it from being considered approximately spherical as is done in many studies of orbital motion around celestial bodies. As a spacecraft approaches an irregular body, the effect of gravitational perturbation on its trajectory becomes increasingly significant as altitude decreases. Thus, for missions aimed at landing, or just a low altitude flyover, the study of trajectories near the asteroid surface is critical. This fact has become evident in recent missions that approached or even landed on the surface of irregular bodies such as the missions of the Japanese Space Agency (JAXA) Hayabusa 1 and Hayabusa 2 [1] or the European Space Agency (ESA) Rosetta mission that studied the comet 67P / Churyumov-Gerasimenko [2-3]. Many other missions for asteroids will take place in the near future, so understanding the dynamics of orbital motion around these bodies is of significant importance.

Thus, this work aims to evaluate, by numerical simulations, the orbits of a spacecraft around asteroid 216 Kleopatra most suitable for approaching the asteroid, in order to minimize the relative velocity between the surface and the vehicle. A polyhedral asteroid volume model, based on radar measurements provided by the Arecibo Observatory, is used to model the non-central gravitational field generated by the asteroid mass distribution. Using the gravitational field model and the simulation environment Spacecraft Trajectory Simulator (STRS) [4-6] approach trajectories were simulated and compared in order to assist in the search for trajectories of minimum altitude and minimum velocity with respect to the asteroid surface.

Asteroid 216 Kleopatra, discovered by Johann Palisa in 1880, has a rather irregular shape with approximate dimensions of 217 x 94 x 81 km, so it can be considered that the study of approximation trajectories with the Kleopatra asteroid is possibly a study of worst case since many other asteroids are not as irregular as Kleopatra. Due to its shape, the gravitational field around the asteroid cannot be considered central, as can be seen in Fig. 1. Thus, a spacecraft approaching the asteroid is subject to orbital disturbances, which may prevent the vehicle from describing its nominal trajectory. In approach and landing maneuvers trajectory deviations can result in very high approach velocities, preventing smooth landing on the asteroid surface. In addition, the rotation of the asteroid represents a further difficulty for missions aimed at soft landing, since due to the irregular shape of the asteroid the relative distance between the surface and the spacecraft varies depending on the orbital plane adopted for the vehicle trajectory.
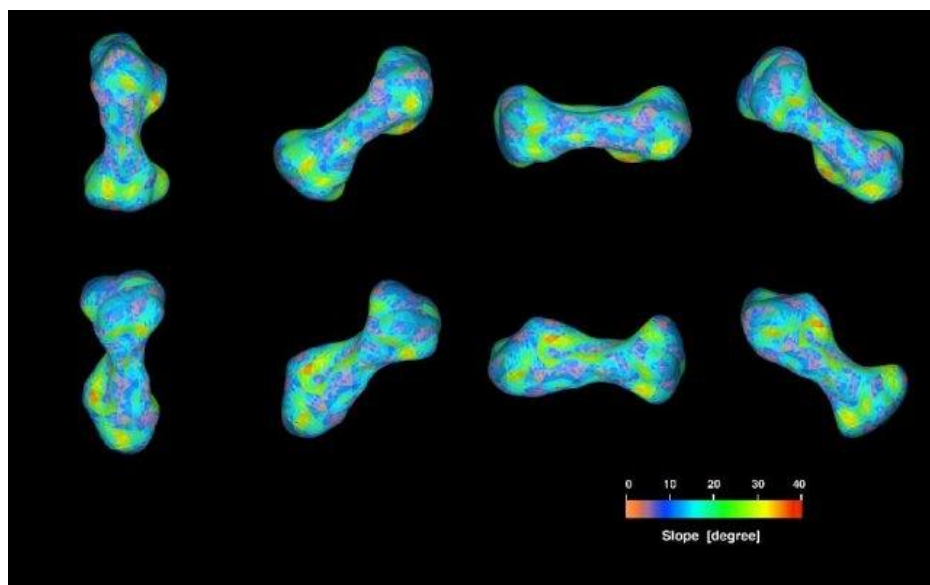

Figure 1. Asteroide 216 Kleopatra [7]

CILAMCE 2019

Proceedings of the XLIbero-LatinAmerican Congress on Computational Methods in Engineering, ABMEC,
Natal/RN, Brazil, November 11-14, 2019

2   Orbital Dynamics

Basically, the orbital motion can be determined by solving the Kepler equation (Eq. 1) at each step of the simulation. Thus, given an initial state and the simulation step, the state can be converted to keplerian elements and propagated to a next step, as illustrated in simplified manner in Fig. 2.

$$M = \sqrt{\frac{\mu}{a^3}}\,(t - T) = u - e\,sin(u) \tag{1}$$

However, the effect of orbital perturbations on the spacecraft's trajectory should be considered. In the literature can be find the classical variational equations that describe the motion of a spacecraft subjected to the action of the disturbing function R [8-10]. These equations are known as Lagrange Planetary Equations (Eq. 2-7) and use the classic orbital elements: semi-major axis (a); eccentricity (e); inclination (i); right ascension of the ascending node (Ω); argument of periapsis (ω); mean anomaly (M). Where n is the mean motion defined by $n = \sqrt{\mu/a^3}$ and μ is the mass of the central body multiplied by the universal gravity constant G.
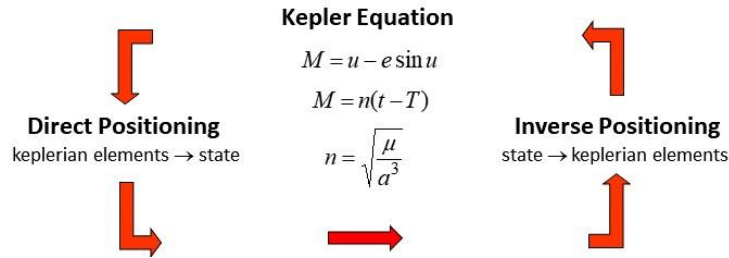

Figure 2. Kepler equation.

$$\frac{da}{dt} = \frac{2}{n\,a}\frac{\partial R}{\partial M} \tag{2}$$

$$\frac{de}{dt} = \frac{-\sqrt{1-e^2}}{n\,a^2\,e}\frac{\partial R}{\partial \omega} + \frac{1-e^2}{n\,a^2\,e}\frac{\partial R}{\partial M} \tag{3}$$

$$\frac{di}{dt} = \frac{-1}{n\,a^2\,\sqrt{1-e^2}\,sin\,i}\frac{\partial R}{\partial \Omega} + \frac{cos\,i}{n\,a^2\,\sqrt{1-e^2}\,sin\,i}\frac{\partial R}{\partial \omega} \tag{4}$$

$$\frac{d\Omega}{dt} = \frac{1}{n\,a^2\,\sqrt{1-e^2}\,sin\,i}\frac{\partial R}{\partial i} \tag{5}$$

$$\frac{d\omega}{dt} = \frac{\sqrt{1-e^2}}{n\,a^2\,e}\frac{\partial R}{\partial e} - \frac{cos\,i}{n\,a^2\,\sqrt{1-e^2}\,sin\,i}\frac{\partial R}{\partial i} \tag{6}$$

$$\frac{dM}{dt} = n - \frac{2}{n\,a}\frac{\partial R}{\partial a} - \frac{1-e^2}{n\,a^2\,e}\frac{\partial R}{\partial e} \tag{7}$$

However, the solution of Lagrange's planetary equations may require a large computational effort to obtain its solution, which may make it difficult or even impossible to simulate the trajectory depending on the complexity of the perturbing function R. In the case of the modeling of the irregular gravitational field around an asteroid, this disturbing function cannot be simplified. Moreover, in the case of using a trajectory control system through the action of the thrusters, the disturbing function must not only consider the environmental disturbances but also consider the action of the control system, making its solution even more difficult. Thus, in the STRS simulator, an equivalent approach to planetary equations were chosen to obtain the orbital element variation rates, but using the state propagation (position and velocity) at each step of the simulation and considering the accelerations disturbances, environmental as well as those applied by the thrusters. The accelerations disturbances are obtained through the disturbance models. That is, the modeling of each perturbation consists in obtaining the disturbing force acting on the vehicle. With the disturbing force, the velocity increments that are inserted in the movement dynamics at each step of the simulation are obtained. Therefore, as with the use of planetary equations, the evolution of orbital elements over time can be obtained as a function of the action of disturbing forces and applied thrust. Thus, the state of the vehicle (position

and velocity) is obtained at each step. By applying the intentional velocity increments and considering the environmental disturbances, it is possible to change the state of the vehicle and thereby modify the keplerian elements of the orbit.

Therefore, as is already clear, the gravitational field of an irregular body cannot be considered as a central force field since its shape does not resemble that of a sphere. In this way the modeling of the gravitational field and the orbital perturbation imposed on the vehicle is fundamental for the simulation of the movement dynamics. In this work the polyhedral model provided by NASA is used to model the irregular body mass distribution [11]. It was considered that in the barycenter (centroid) of each polyhedron is allocated a mass concentration equivalent to the mass of the respective polyhedron. In this way, the gravitational force applied to the vehicle due to each of the mass concentrations can be calculated. By effecting the integral of all forces the resulting gravitational force is obtained. The comparison between this resultant with the gravitational force that would be generated if the force field were central provides the disturbing force that is applied to the vehicle at each step of the simulation [12-13], as illustrated in Fig. 2.

Figure 3. Orbital dynamics considering the asteroid discretization.

That is, the asteroid is decomposed into a set of tetrahedra with one of the common vertices located at the center of mass of the body [14-15]. The mass of each tetrahedron is calculated and from the vertex coordinates the tetrahedron centroid coordinates can be obtained. The centroid is the center of mass of a solid. The mass of a solid with a volume V and density function $\rho(x,y,z)$ is given by Eq. 8.

$$m = \iiint \rho(x, y, z) dV \tag{8}$$

The tetrahedron centroid coordinates can be obtained using the following expressions (Eq. 9-11).

$$\bar{x} = \frac{\iiint x\, \rho(x,y,z) dV}{m} \tag{9}$$

$$\bar{y} = \frac{\iiint y\, \rho(x,y,z) dV}{m} \tag{10}$$

$$\bar{z} = \frac{\iiint z\, \rho(x,y,z) dV}{m} \tag{11}$$

Considering the centroid coordinates of all tetrahedra and their respective masses, in order to consider that all tetrahedron mass is concentrated in the centroid, the gravitational pull exerted on the vehicle by each mass concentration can be calculated. Thus, the problem consist in given the vehicle positions and the mass concentrations, and all masses involved, calculate the gravitational force resulting from the action of all mass concentrations that modeling the asteroid.

From Fig. 4 the vectors that provide the position with respect to the center of mass of the asteroid, to the vehicle and to a generic mass concentration (i), can be obtained. Eq. 12 to 17 provide these position vectors. Eq. 18 to 24 provide the gravitational forces involved. $F_{gi_x}\hat{\imath}$, $F_{gi_y}\hat{\jmath}$ and $F_{gi_z}\hat{k}$ are the components of the gravitational force generated by mass concentration. $F_{gT_x}\hat{\imath}$, $F_{gT_y}\hat{\jmath}$ and $F_{gT_z}\hat{k}$ are the components of the total gravitational force generated by the asteroid. $\overrightarrow{F_c}$ is the vector representing the central field gravitational force. $\overrightarrow{F_{gT}}$ is the vector representing the actual gravitational force generated

by the asteroid. Therefore, the difference between $\overrightarrow{F_{gT}}$ and $\overrightarrow{F_c}$ provides the vector $\overrightarrow{F_p}$ that represents the disturbing force due to irregular mass distribution of the asteroid [16-17].
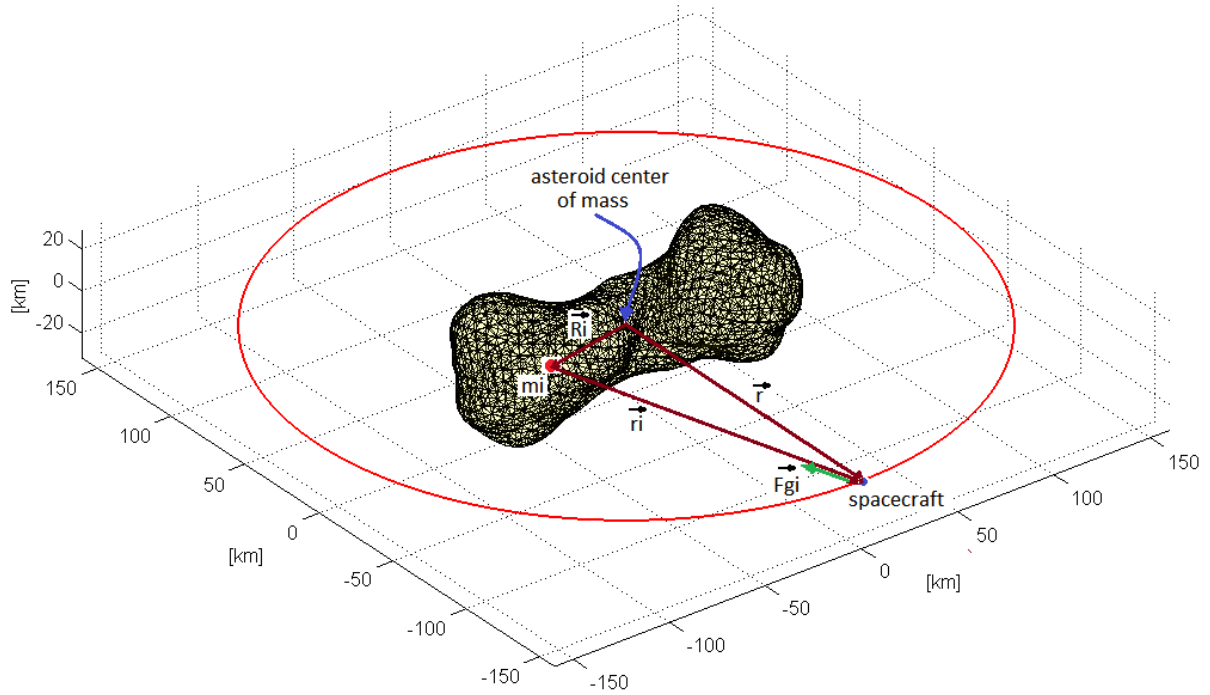

Figure 4. Position vectors.

$$\overrightarrow{R_i} + \overrightarrow{r_i} = \vec{r} \tag{12}$$

$$\overrightarrow{R_i} = R_{ix}\hat{\imath} + R_{iy}\hat{\jmath} + R_{iz}\hat{k} \tag{13}$$

$$\overrightarrow{r_i} = r_{ix}\hat{\imath} + r_{iy}\hat{\jmath} + r_{iz}\hat{k} \tag{14}$$

$$\vec{r} = r_x\hat{\imath} + r_y\hat{\jmath} + r_z\hat{k} \tag{15}$$

$$\overrightarrow{r_i} = (r_x - R_{ix})\hat{\imath} + (r_y - R_{iy})\hat{\jmath} + (r_z - R_{iz})\hat{k} \tag{16}$$

$$r_i = \sqrt{(r_x - R_{ix})^2 + (r_y - R_{iy})^2 + (r_z - R_{iz})^2} \tag{17}$$

$$F_{gi_x}\hat{\imath} = -\frac{G\, m_i\, m_{sp}}{r_i^2}\frac{(r_x - R_{ix})}{r_i}\hat{\imath} \tag{18}$$

$$F_{gi_y}\hat{\jmath} = -\frac{G\, m_i\, m_{sp}}{r_i^2}\frac{(r_y - R_{iy})}{r_i}\hat{\jmath} \tag{19}$$

$$F_{gi_z}\hat{k} = -\frac{G\, m_i\, m_{sp}}{r_i^2}\frac{(r_z - R_{iz})}{r_i}\hat{k} \tag{20}$$

$$F_{gT_x}\hat{\imath} = \sum_{i=1}^{N} F_{gi_x}\hat{\imath} \tag{21}$$

$$F_{gT_y}\hat{\jmath} = \sum_{i=1}^{N} F_{gi_y}\hat{\jmath} \tag{22}$$

$$F_{gT_z}\hat{k} = \sum_{i=1}^{N} F_{gi_z}\hat{k} \tag{23}$$

$$\overrightarrow{F_p} = \overrightarrow{F_{gT}} - \overrightarrow{F_c} \tag{24}$$

3   Results

Seven simulations were performed, each consisting of two parts: The simulation (a), lasting three earth days, does not consider the action of the control system, thus the orbit of the vehicle evolves significantly under the action of the disturbance. Simulation (b), lasting one orbit around the asteroid, considers the action of the control system to mitigate the effect of the disturbance, in this case the trajectory remains close to a circular orbit. The trajectories described by the spacecraft can be seen in Fig. 5 to 18. The various simulations were performed for different orbital inclinations, ranging from zero to 90º. The initial orbital elements considered in all simulations were as follows: $a = 160$ km; $e = 0.000001$; $\Omega = 90º$; $\omega = 180º$; $M = 0$; $i = 0$ (Sim. 1); $i = 15º$ (Sim. 2); $i = 30º$ (Sim. 3); $i = 45º$ (Sim. 4); $i = 60º$ (Sim. 5); $i = 75º$ (Sim. 6); $i = 90º$ (Sim. 7). In each simulation, the vehicle's altitude and velocity relative to the asteroid surface were verified. However, in this study, no orbital maneuvers were performed with the intention of landing. Prior to landing, the closest orbits to the surface should be assessed due to the irregular shape of the asteroid, and the relative vehicle-surface velocity at the closest approach should be assessed.

Figure 5. Trajectory - Sim. 1a: without control.

Figure 6. Trajectory - Sim. 1b: with control.

Figure 7. Trajectory - Sim. 2a: without control.

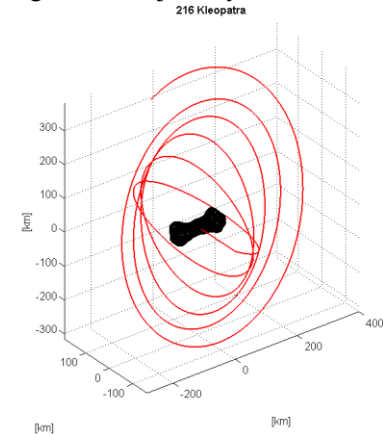Figure 8. Trajectory - Sim. 2b: with control.

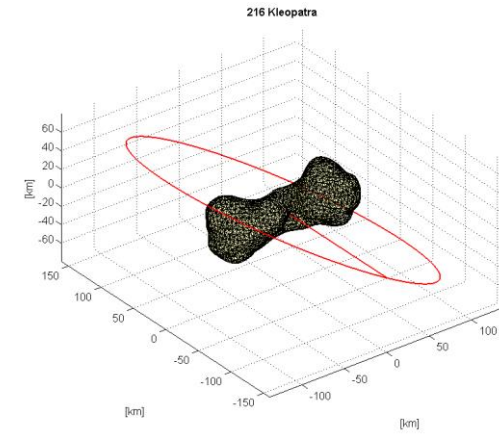Figure 9. Trajectory - Sim. 3a: without control.
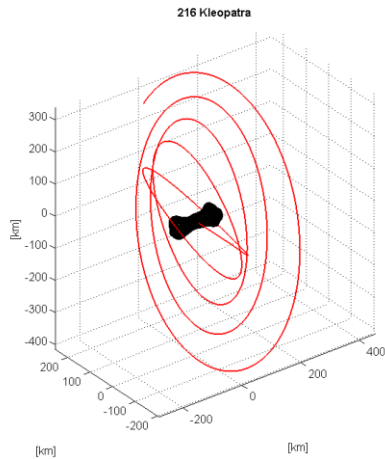

Figure 10. Trajectory - Sim. 3b: with control.

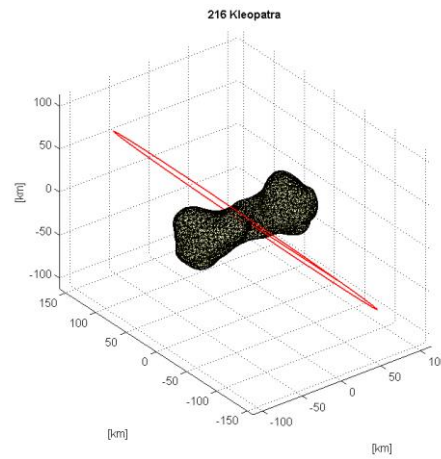Figure 11. Trajectory - Sim. 4a: without control.

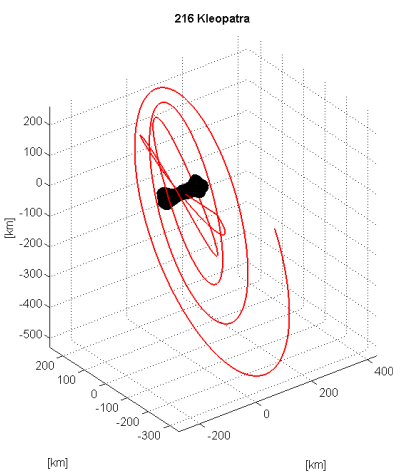Figure 12. Trajectory - Sim. 4b: with control.

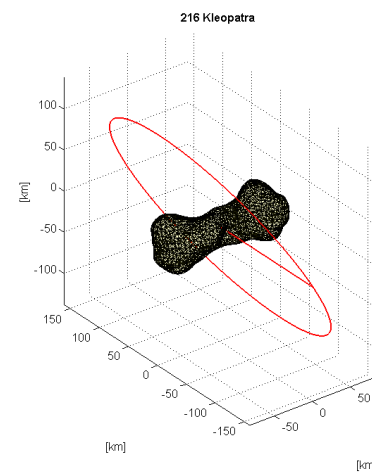Figure 13. Trajectory - Sim. 5a: without control.

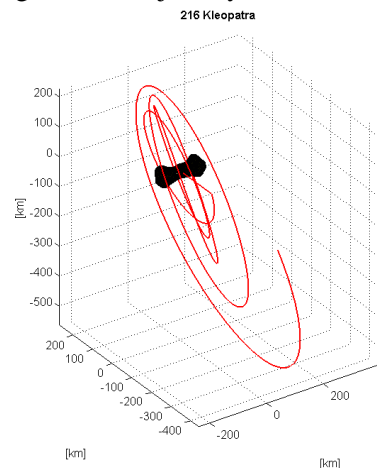Figure 14. Trajectory - Sim. 5b: with control.

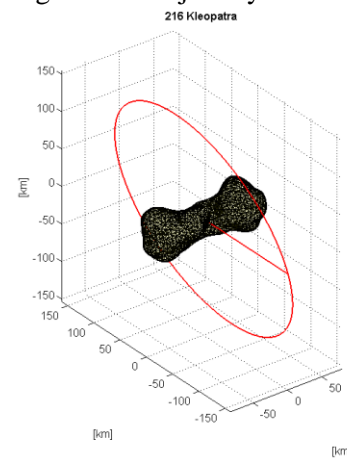Figure 15. Trajectory - Sim. 6a: without control.

Figure 16. Trajectory - Sim. 6b: with control.

In the figures of the simulations in which the performance of the control system was not considered, it is evident that the orbit undergoes major variations due to the disturbance generated by the gravitational field of the asteroid. In simulations 1a and 2a the orbit eccentricity approached the eccentricity of a parabolic orbit and for this reason the simulation was interrupted at e = 0.95. If the simulation proceeded the orbit would become hyperbolic, and for the simulations 1a and 2a, the vehicle would collide with the surface. In the other simulations, during the evaluated period, the vehicle did not collide with the asteroid and it was possible to finish the simulations after three terrestrial days. The graphs showing the evolution of orbital elements for simulations 1 and 7 can be seen in Fig. 19 to 35, and the data related to all simulations can be seen in Table 1 to 14.
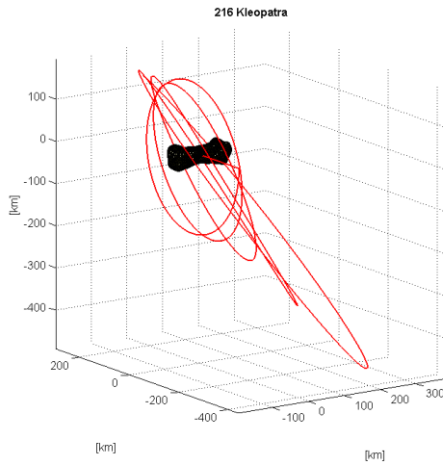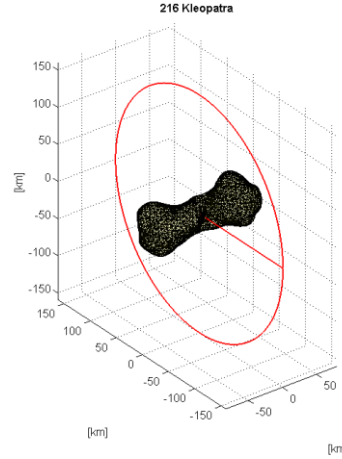
Figure 17. Trajectory - Sim. 7a: without control.

Figure 18. Trajectory - Sim. 7b: with control.

Table 1. Simulation 1a without control of the trajectory ($i_{initial} = 0$)

Simulation time	43410 s - simulation interrupted for $e = 0.95$
Minimum altitude	20.003 km at 43410 s
Velocity related to the asteroid surface	79.1687 m/s

Table 2. Simulation 1b with control of the trajectory ($i_{initial} = 0$)

Simulation time	22860 s - one orbit
Minimum altitude 1	80.0355 km at 3015 s
Velocity related to the asteroid surface at mim. alt. 1	44.8937 m/s
Minimum altitude 2	76.288 km at 8340 s
Velocity related to the asteroid surface at mim. alt. 2	44.8935 m/s
Sum of the disturbance velocity	79.9358 m/s

Table 3. Simulation 2a without control of the trajectory ($i_{initial} = 15°$)

Simulation time	10540 s - simulation interrupted for $e = 0.95$
Minimum altitude	7.4071 km at 10540 s
Velocity related to the asteroid surface	84.1961 m/s

Table 4. Simulation 2b with control of the trajectory ($i_{initial} = 15°$)

Simulation time	22860 s - one orbit
Minimum altitude 1	84.0779 km at 3195 s
Velocity related to the asteroid surface at mim. alt. 1	44.8631 m/s
Minimum altitude 2	78.0253 km at 8252.5 s
Velocity related to the asteroid surface at mim. alt. 2	44.8630 m/s
Sum of the disturbance velocity	73.9994 m/s

Table 5. Simulation 3a without control of the trajectory ($i_{initial} = 30°$)

Simulation time	259200 s - 3 days
Minimum altitude	105.4387 km at 2137.5 s
Maximum altitude	387.0771 km at 117340 s
Velocity related to the asteroid surface at min. altitude	46.1267 m/s

Table 6. Simulation 3b with control of the trajectory ($i_{initial} = 30°$)

Simulation time	22860 s - one orbit
Minimum altitude 1	88.6904 km at 3295 s
Velocity related to the asteroid surface at mim. alt. 1	44.7733 m/s
Minimum altitude 2	83.4906 km at 8230 s
Velocity related to the asteroid surface at mim. alt. 2	44.7733 m/s
Sum of the disturbance velocity	61.7602 m/s

Table 7. Simulation 4a without control of the trajectory ($i_{initial} = 45°$)

Simulation time	259200 s - 3 days
Minimum altitude	112.5488 km at 1960 s
Maximum altitude	470.8944 km at 11310 s
Velocity related to the asteroid surface at mim. altitude	44.4813 m/s

Table 8. Simulation 4b with control of the trajectory ($i_{initial} = 45°$)

Simulation time	22860 s - one orbit
Minimum altitude 1	96.7221 km at 3405 s
Velocity related to the asteroid surface at mim. alt. 1	44.6301 m/s
Minimum altitude 2	93.6211 km at 7997.5 s
Velocity related to the asteroid surface at mim. alt. 2	44.6302 m/s
Sum of the disturbance velocity	51.2328 m/s

Table 9. Simulation 5a without control of the trajectory ($i_{initial} = 60°$)

Simulation time	259200 s - 3 days
Minimum altitude	122.5727 km at 1730 s
Maximum altitude	560.2079 km at 12025 s
Velocity related to the asteroid surface at mim. altitude	43.2509 m/s

Table 10. Simulation 5b with control of the trajectory ($i_{initial} = 60°$)

Simulation time	22860 s - one orbit
Minimum altitude 1	107.5401 km at 3355 s
Velocity related to the asteroid surface at mim. alt. 1	44.4431 m/s
Minimum altitude 2	107.5020 km at 7882.5 s
Velocity related to the asteroid surface at mim. alt. 2	44.4441 m/s
Sum of the disturbance velocity	47.4400 m/s

Table 11. Simulation 6a without control of the trajectory ($i_{initial} = 75°$)

Simulation time	259200 s - 3 days
Minimum altitude	127.3374 km at 13912.5 s
Maximum altitude	608.2321 km at 118910 s
Velocity related to the asteroid surface at mim. altitude	43.9453 m/s

Table 12. Simulation 6b with control of the trajectory ($i_{initial} = 75°$)

Simulation time	22860 s - one orbit
Minimum altitude 1	120.7963 km at 3482.5 s
Velocity related to the asteroid surface at mim. alt. 1	44.2260 m/s
Minimum altitude 2	127.0861 km at 7542.5 s
Velocity related to the asteroid surface at mim. alt. 2	44.2275 m/s
Sum of the disturbance velocity	48.2844 m/s

Table 13. Simulation 7a without control of the trajectory ($i_{initial} = 90°$)

Simulation time	259200 s - 3 days
Minimum altitude	130.2773 km at 14577.5 s
Maximum altitude	565.2426 km at 106510 s
Velocity related to the asteroid surface at mim. altitude	43.8304 m/s

Table 14. Simulation 7b with control of the trajectory ($i_{initial} = 90°$)

Simulation time	22860 s - one orbit
Minimum altitude 1	131.0896 km at 0 s
Velocity related to the asteroid surface at mim. alt. 1	43.9999 m/s
Minimum altitude 2	127.0269 km at 11285 s
Velocity related to the asteroid surface at mim. alt. 2	44.0001 m/s
Sum of the disturbance velocity	49.1311 m/s

From the analysis of the tables we can see that in simulations (a) the greatest approximations occurred for simulations 1a and 2a with altitudes of 20.0030 km and 7.471 km respectively. However, in these simulations the vehicle would hit the asteroid with a velocity with respect to the surface around 80 m/s, so the measured altitude were the altitudes at the moment the simulation was stopped. Analyzing the other simulations (a), where the simulation time was three days, it is verified that the minimum altitude occurred in the simulation 3a with ground velocity of 46.1267 m / s. However, in the simulation 5a the minimum altitude was 122.5727 km for a ground velocity of 43.2509 m/s, the lowest speed of all simulations performed.

For simulations (b), when the control system was acting, the minimum altitude occurred in simulation 1b with an altitude of 76.2880 km and a ground velocity of 44.8935 m/s. However, the sum of the disturbing velocity increments, value analogous to the integral of perturbation to which the vehicle is subjected, was 79,935 m/s. This is the largest value of all simulations. To mitigate the effect of the disturbance the control system must act to apply a similar velocity increment, so the higher the sum of the disturbing increments, the greater the fuel expenditure to mitigate the disturbance effect.

The optimum value obtained for the sum of the disturbing increments occurred in simulation 5b with the value of 47.4400 m/s, but the minimum altitude in this simulation was 107.5020 km. The ground velocities at the minimum altitude were around 44 m/s in all simulations of the case (b).

Therefore, it is clear that selecting the trajectory with minimum altitude, minimum ground velocity and minimum fuel consumption for mitigating the effects of the disturbance, is not an easy task as the objectives are conflicting [18-20]. Thus, it is necessary to apply a multi-objective optimization approach, as applied in [21-22].
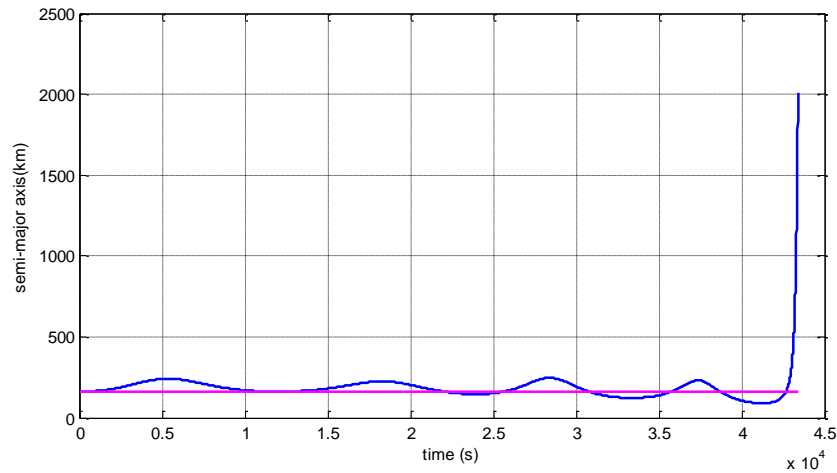
Figure 19. Semi major-axis – Simulation 1a: without control of the trajectory
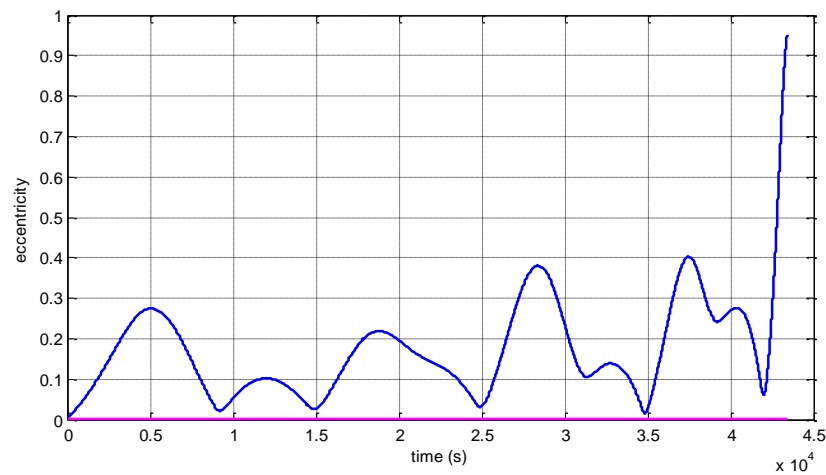

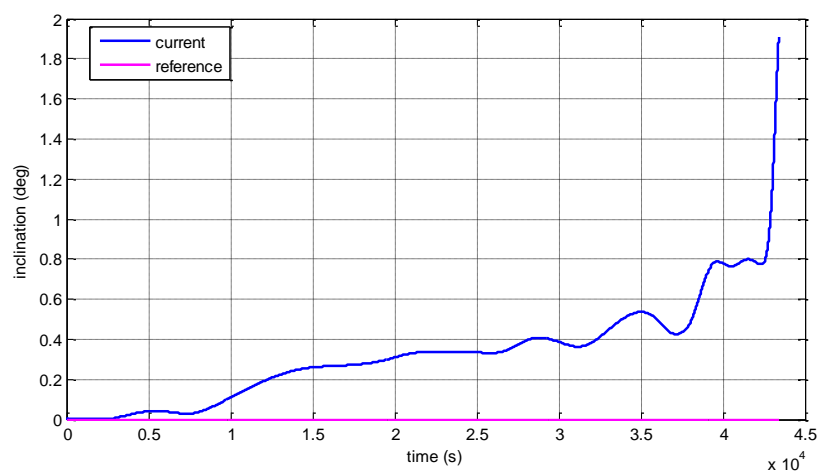Figure 20. Eccentricity – Simulation 1a: without control of the trajectory

Figure 21. Inclination – Simulation 1a: without control of the trajectory
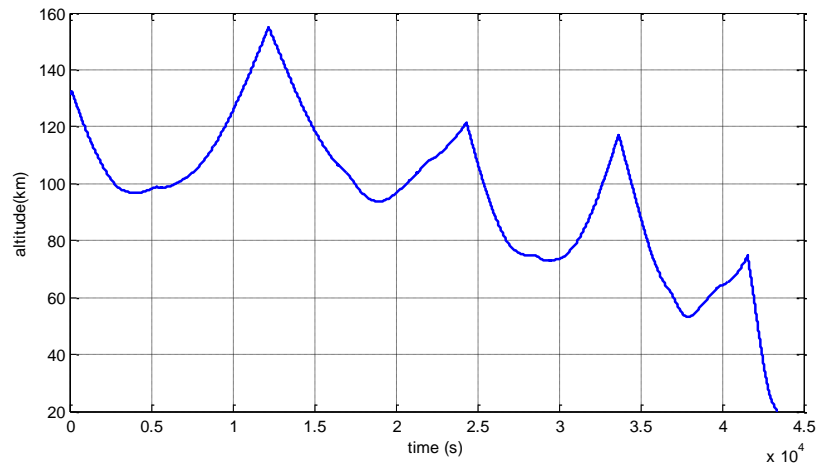
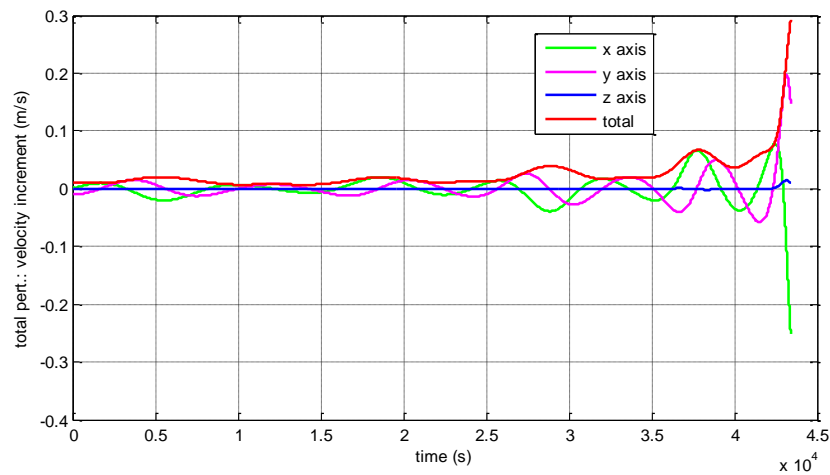Figure 22. Altitude – Simulation 1a: without control of the trajectory

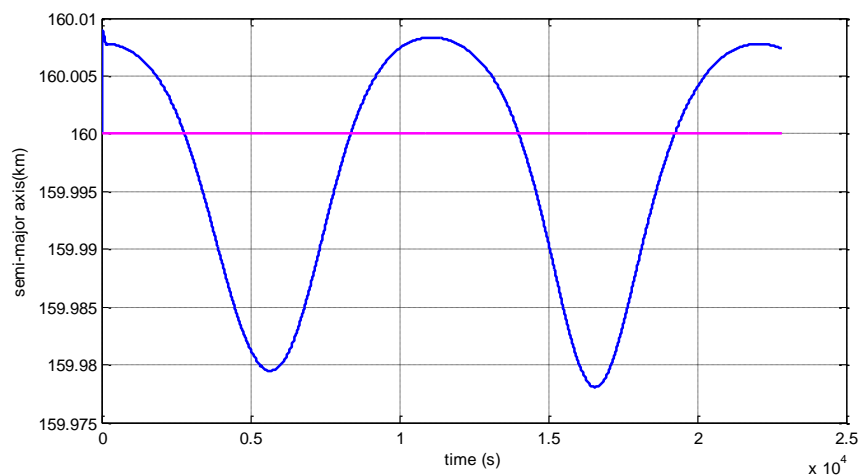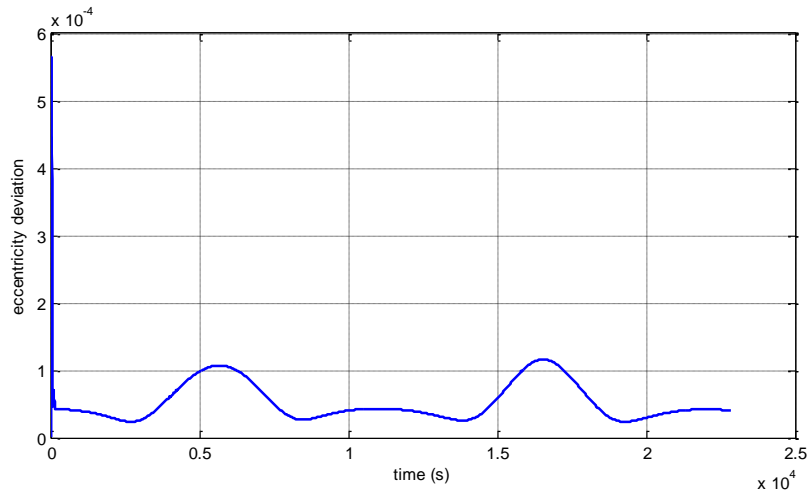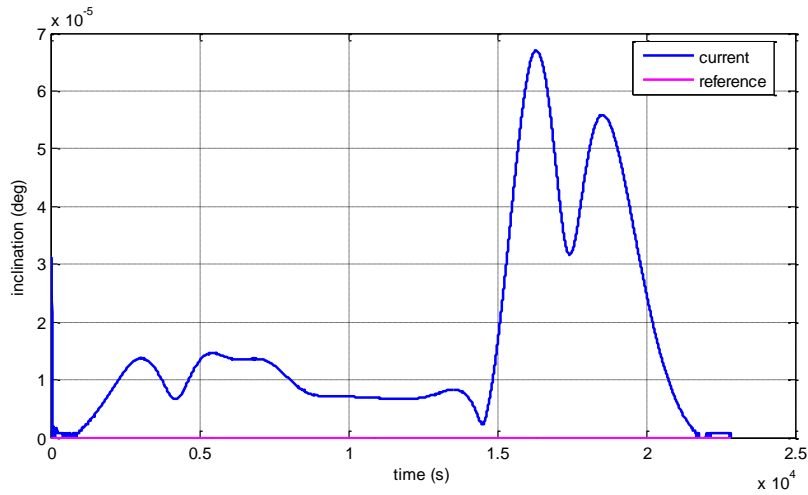Figure 23. Vel. increment due to the disturbances – Simulation 1a: without control of the trajectory

Figure 24. Semi major-axis – Simulation 1a: with control of the trajectory

Figure 25. Eccentricity – Simulation 1b: with control of the trajectory

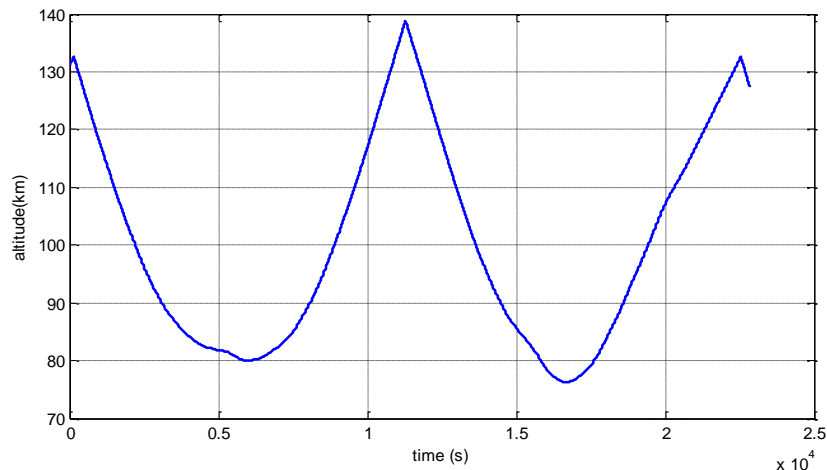Figure 26. Inclination – Simulation 1b: with control of the trajectory

Figure 27. Altitude – Simulation 1b: with control of the trajectory
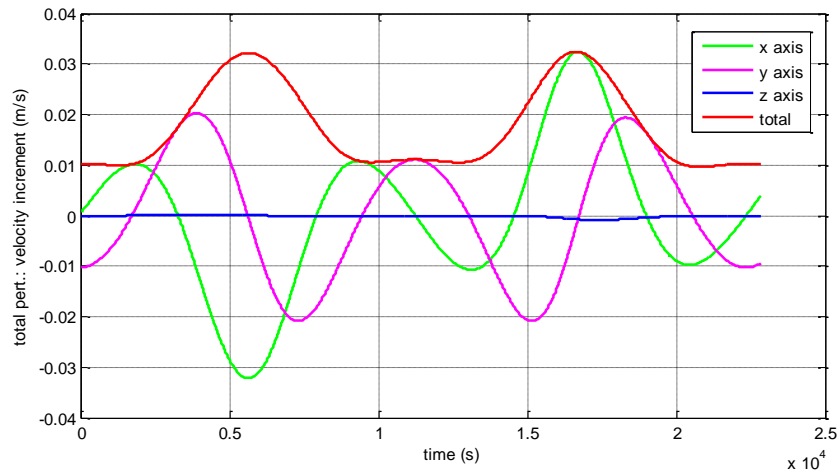
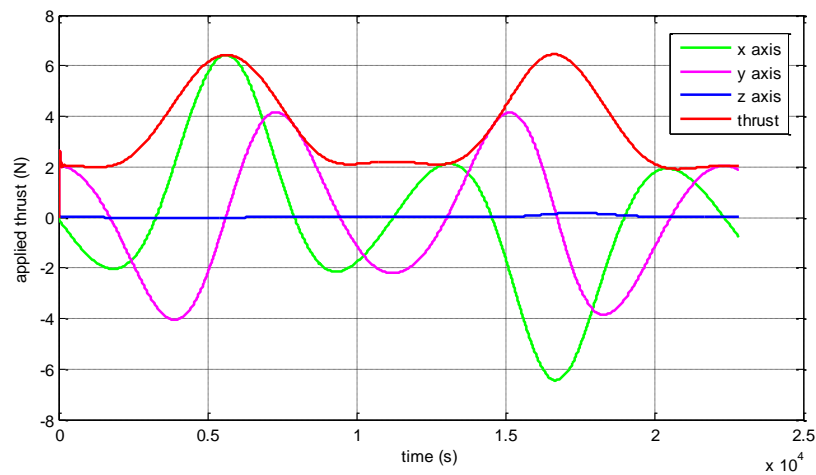Figure 28. Disturbances velocity increment– Simulation 1b: with control of the trajectory

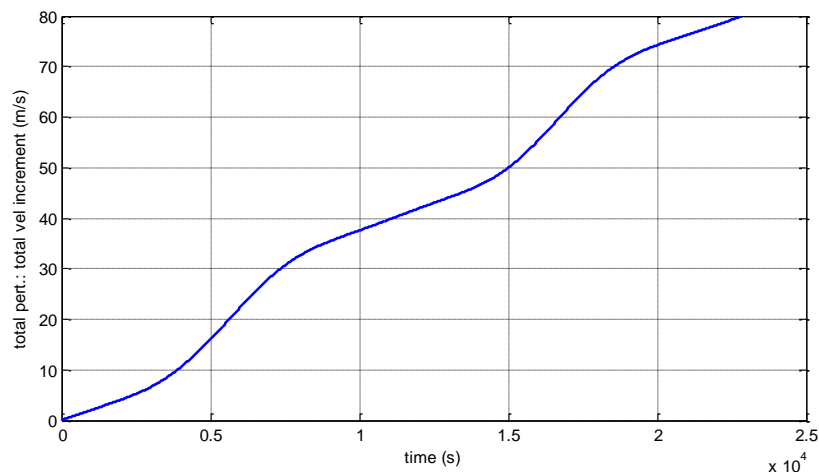Figure 29. Applied thrust – Simulation 1b: with control of the trajectory

Figure 30. Sum of disturbances velocity increment – Simulation 1b: with control of the trajectory
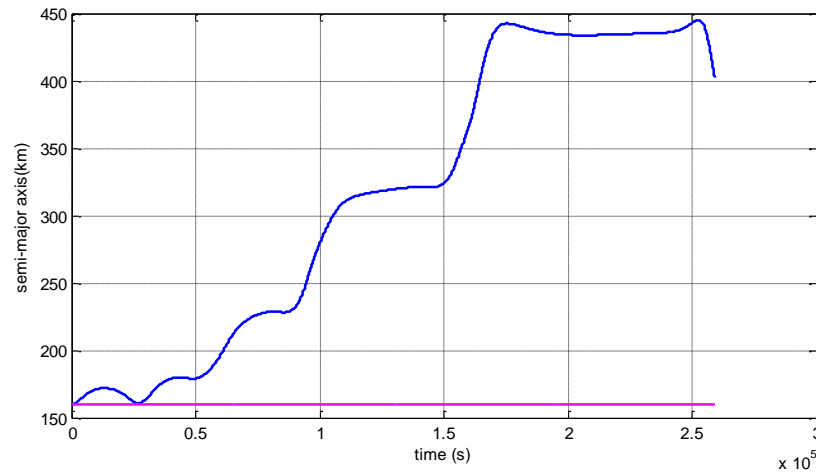
Figure 31. Semi major-axis – Simulation 7a: without control of the trajectory
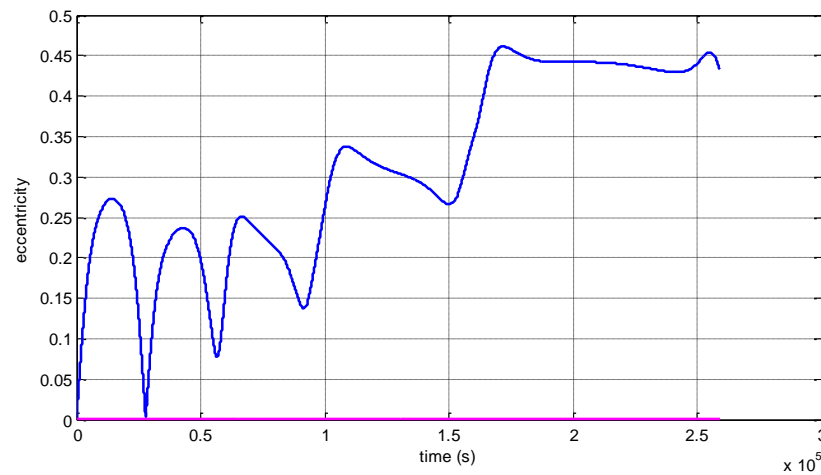

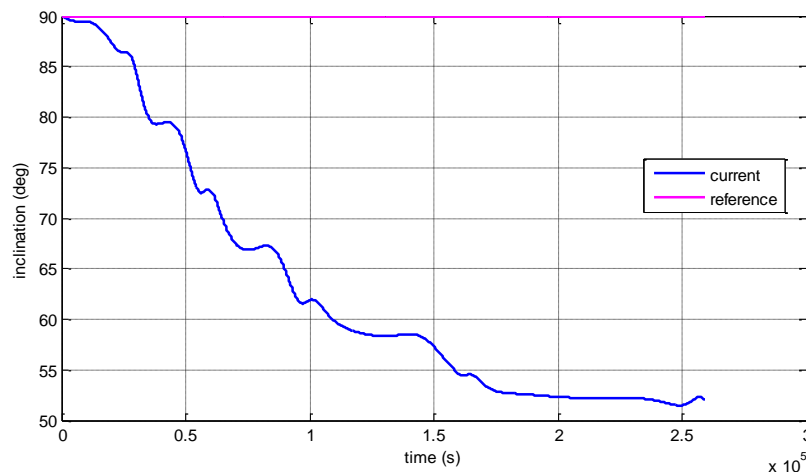Figure 32. Eccentricity – Simulation 7a: without control of the trajectory

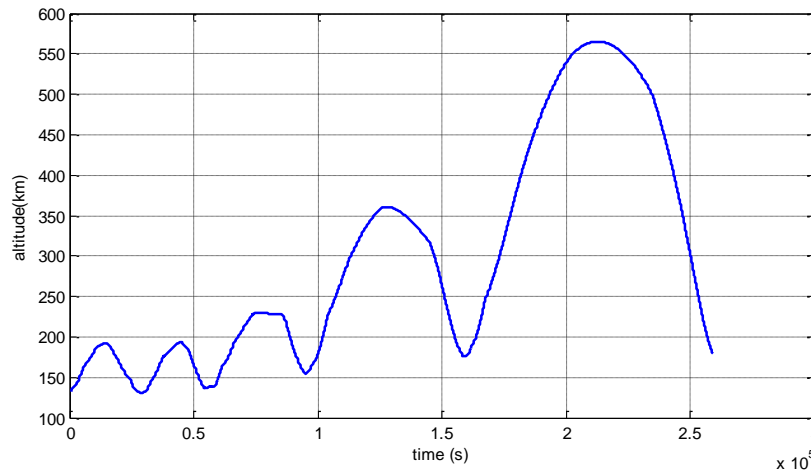Figure 33. Inclination – Simulation 7a: without control of the trajectory

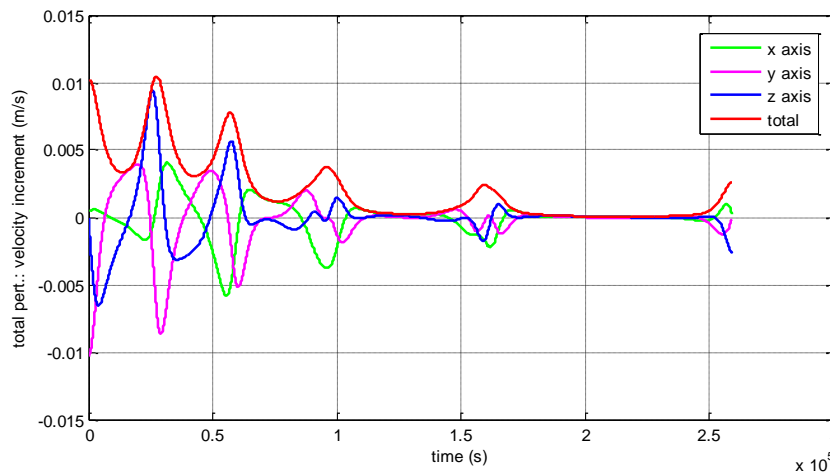Figure 34. Altitude – Simulation 7a: without control of the trajectory

Figure 35. Vel. increment due to the disturbances – Simulation 7a: without control of the trajectory

4   Conclusion

The simulations showed that due to the irregular shape of the asteroid the vehicle approaches the surface even when using a practically circular orbit. The maximum approach occurred for inclinations of 0º and 15º, when the vehicle reached an altitude of approximately 76 km and 78 km respectively. However, it should be noted that the problem of the approaching and landing on an asteroid has no single solution, as there are various combinations of the initial orbit and asteroid positioning. As altitude is a function of the asteroid relief, besides being a function of the adopted trajectory, it is of fundamental importance to use simulations similar to those performed in this study as a way to predict the speed with which the vehicle approaches the surface. Thus, this work represents the starting point for the study of landing procedures on the surface of an asteroid.

References

[1] http://www.jspec.jaxa.jp/e/activity/hayabusa2.html

[2] Seidensticker, K. J.; Möhlmann; Apathy, I.; Schmidt, W.; Thiel, K.; Arnold, W.; Fischer, H.-H.; Kretschmer, M.; Madlener, D. *Sesame – An Experiment of the Rosetta Lander Philae: Objectives and General Design*. Space Science Reviews. 128. 2007. doi:10.1007/s11214-006-9118-6

[3] Scheeres, D. J., Marzari, F., Tomasella, L., & Vanzani, V. (1998). ROSETTA mission: satellite orbits around a cometary nucleus. Planetary and Space Science, 46(6), 649-671.

[4] Rocco, E. M., *Perturbed Orbital Motion with a PID Control System for the Trajectory*, XIV Colóquio Brasileiro de Dinâmica Orbital, Águas de Lindóia, 17 a 21 de novembro de 2008.

[5] Rocco, E. M. *Analysis of the deviations of the trajectory due to the terrestrial albedo applied to some scientific missions*. Proceedings of the International Conference on Mathematical Problems in Engineering, Aerospace and Sciences, Genova, Italy, 2008.

[6] Rocco, E.M., *Automatic correction of orbital elements using continuous thrust controlled in closed loop*. Journal of Physics: Conference Series, 465, 2013 doi:10.1088/1742-6596/465/1/012027.

[7] Ostro, S.J., R.S. Hudson, M.C. Nolan, J.-L. Margot, D.J. Scheeres, D.B. Campbell, C. Magri, J.D. Giorgini, and D.K. Yeomans. *Radar observations of asteroid 216 Kleopatra*. Science 288, 836-839, 2000.

[8] Kovalevski, J. *Introduction to celestial mechanics*. New York, NY, Springer Verlag, 1967.

[9] Bate, R.R., Mueller, D.D., White, J.E. *Fundamentals of Astrodynamics*. Dover Publications, New York, 1971.

[10] Battin, R. H., *An Introduction to the Mathematics and Methods of astrodynamics*, Rev. ed. AIAA Educational Series, Reston, 1999.

[11] Stooke, P., "Small Body Shape Models. EAR-A-5-DDR-STOOKE-SHAPE-MODELS-V1.0." NASA Planetary Data System, 2002.

[12] Gonçalves, L. D.; Rocco, E. M.; de Moraes, R. V. *Trajectories in the vicinity of Fobos aiming overflight and approach.* Colóquio Brasileiro de Dinâmica Orbital, 2016.

[13] Rocco E M; Gonçalves L D; Moraes R V *Orbital maneuvers in the non-central gravitational field of Phobos perturbed by the gravitational attraction due to Mars, Sun and Deimos*. In: 27th Space Flight Mechanics Meeting, San Antonio. Proceedings of the 27th Space Flight Mechanics Meeting, 2017.

[14] Werner R. A *The gravitational potential of a homogeneous polyhedron or don't cut corners*. Celestial Mechanics and Dynamical Astronomy, vol. 59, no. 3, p. 253-278, 1994

[15] Mota, M. L. *Modelo do campo gravitacional de um corpo com distribuição de massa irregular utilizando o método da expansão do potencial em série e determinação de seus coeficientes dos harmônicos esféricos*. PhD Thesis, Instituto Nacional de Pesquisas Espaciais, 2017.

[16] Venditti, F. C. F. *Orbital maneuvers around irregular shaped bodies*. PhD Thesis, Instituto Nacional de Pesquisas Espaciais 2013.

[17] Venditti, F. C. F.; Rocco, E. M. *Modeling asteroids to assist in orbiting and landing missions.* Advances in the Astronautical Sciences, vol. 162. Proceedings of the AAS/AIAA Astrodynamics Specialist Conference, Washington, USA, 2017.

[18] Scheeres, D.J., Ostro, S.J., Hudson, R.S., and Werner, R.A. *Orbits Close to Asteroid 4769 Castalia*, Icarus, Vol 121, pp. 67-87, 1996.

[19] Scheeres, D. J. *Close Proximity operations for implementing mitigation strategies*. 2004 Planetary Defense Conference: Protecting Earth from Asteroids. Orange County:[sn], 2004.

[20] Scheeres, D. J; *Orbit Mechanics about Small Asteroids*. Acta Astronautica, 2012.

[21] Rocco, E. M.; Souza, M. L. O.; Prado, A.F.B.A. *Station Keeping of Constellations Using Multiobjective Strategies*. Mathematical Problems in Engineering, v. 2013, p. 1-15, 2013. doi:10.1155/2013/476451

[22] Venditti, F. C. F.; Rocco, E.M.; Prado, A. F. B. A.; Suhkanov, A. *Gravity-assisted maneuvers applied in the multi-objective optimization of interplanetary trajectories*. Acta Astronautica, v. 67, p. 1255-1271, 2010